MDPI

Article

Numerical Simulation of the Effects of Reduced Gravity, Radiation and Magnetic Field on Heat Transfer Past a Solid Sphere Using Finite Difference Method

Amir Abbas [1], Muhammad Ashraf [2], Ioannis E. Sarris [3], Kaouther Ghachem [4], Taher Labidi [5], Lioua Kolsi [6,7,*] and Hafeez Ahmad [8]

1   Department of Mathematics, Faculty of Science, University of Gujrat, Sub-Campus, Mandi Bahauddin 50400, Pakistan
2   Department of Mathematics, Faculty of Science, University of Sargodha, Sargodha 40100, Pakistan
3   Department of Mechanical Engineering, University of West Attica, 250 Thivon & P. Rall Str., Egaleo, 12244 Athens, Greece
4   Department of Industrial Engineering and Systems, College of Engineering, Princess Nourah Bint Abdulrahman University, P.O. Box 84428, Riyadh 11671, Saudi Arabia
5   Department of Software Engineering, College of Computer Engineering and Sciences, Prince Sattam Bin Abdulaziz University, P.O. Box 151, Al-Kharj 11942, Saudi Arabia
6   Department of Mechanical Engineering, College of Engineering, University of Ha'il, Ha'il City 81451, Saudi Arabia
7   Laboratory of Metrology and Energy Systems, Department of Energy Engineering, University of Monastir, Monastir 5000, Tunisia
8   Department of Statistics, School of Quantitative Sciences, University of Utara, Kedah 06010, Malaysia
*   Correspondence: lioua_enim@yahoo.fr

Abstract: The current study deals with the reduced gravity and radiation effects on the magneto-hydrodynamic natural convection past a solid sphere. The studied configuration is modeled using coupled and nonlinear partial differential equations. The obtained model is transformed to dimensionless form using suitable scaling variables. The finite difference method is adopted to solve the governing equation and determine the velocity and temperature profiles in addition to the skin friction coefficient and Nusselt number. Furthermore, graphic and tabular presentations of the results are made. The verification of the numerical model is performed by comparing with results presented in the literature and a good concordance is encountered. The main objective of this investigation is to study the effect of the buoyancy force caused by the density variation on natural convective heat transfer past a solid sphere. The results show that the velocity increases with the reduced gravity parameter and solar radiation but decreases with Prandtl number and magnetic field parameter. It is also found that the temperature increases the with solar radiation and magnetic field but decreases with the reduced gravity parameter and Prandtl number.

Keywords: reduced gravity; magnetohydrodynamics; natural convection; solar radiation; finite difference method; sphere

1. Introduction

Natural convection has become the interest of researchers and engineering due to its manifestation in several natural phenomena and engineering applications. This can be seen in the plume rising from the hot air from fire, oceanic currents, etc. Its principal applications in the industrial field are natural cooling and ventilation without the assistance of fans. The physics of reduced gravity is of great interest and the spherical-shaped components are significant in industry and engineering applications. Potter and Rily [1] investigated the free convection model for high Grashof number values. For fixed values of Prandtl and Grashof numbers, Riley [2] investigated natural convection around a stationary

sphere. Heat Transfer process due to heated bar under the consideration of reduced gravity influence has been carried out by Kay [3]. An oscillatory heat transport process past a stationary sphere was performed by Ashraf et al. [4]. Ashraf and Fatima [5] numerically solved the unsteady fluid flow and heat transfer along a sphere by considering the fluid dissipation effect. Ashraf et al. [6] considered the nanofluid free convection in the plume region above a stationary sphere. The effects of thermophoretic transportation on convective heat transfer by taking different fluid characteristics along a sphere have been explored in [7–12]. Ahmad et al. [13] used the finite difference method to numerically study the combined effect of chemical reaction and convective heat transfer along a curved surface. Abbas et al. [14] numerically studied the MHD Sakiadis flow using variable density influence on an inclined surface. Rashad et al. [15] analyzed the energy transport in a nanofluid due to convection along cylindrical geometry inserted in porous media. Khan et al. [16] studied the MHD free convection in a vapor plume formed as a result of a fluid eruption while considering the effect of heat generation.

Bulinda et al. [17] investigated the magnetohydrodynamic free convective flow process along a corrugated vibrating bottom surface with a focus on the effects of Hall currents. Molla et al. [18] considered the impact of varying conductivity on the natural convection over a sphere immersed in quiescent fluid. Alwawi et al. [19] presented a study on the MHD natural convection flow of a Casson nanofluid around a solid sphere. Jenifer et al. [20] proposed a model of unsteady mixed convection past a sphere with the consideration of magnetic field and variable fluid property effects. Ahmad et al. [21] considered the chemically reacting natural convection past a curved surface with varying of the thermal conductivity and dynamic viscosity. Salleh et al. [22] considered the mixed convective flow around a sphere by considering the Newtonian heating effect. The effects of varying viscosity and chemical reaction on the natural convection process were investigated by Molla and Hossain [23]. Chamkha et al. [24] numerically modeled a non-Darcy heat transfer of a nanofluid past a porous vertical cone inserted in a permeable medium. Chamkha [25] investigated the MHD double diffusion natural convection past a sphere. Sparrow and Gregg [26] studied the free and forced convection flows over a flat plate for low Prandtl number values. Zhang et al. [27] studied the thermal-mechanical coupling propagation and transient thermal fracture in multilayer coatings. Liu et al. [28] considered a 3D solid-air model to simulate heat and mass transfer in vertical double tube heat exchangers. Some other relevant studies related to the current subject can be found in the literature [29–45].

Based on the above described literature review, it can be concluded that combined effects of magnetohydrodynamic, reduced gravity, and solar radiation on natural convection past a sphere have not been the subject of any study before the present attempt. The developed model and solution procedure are presented in the next sections. The results are displayed in graphs and tables with a detailed discussion based on physical interpretations.

2. Problem Analysis

The studied configuration (Figure 1) corresponds to a two-dimensional viscous, steady, and incompressible flow past a stationary sphere in the presence of an external horizontal magnetic field. Coordinates along and normal to the flow are (x, y). Temperature of a surface is T_w and free stream temperature is T_∞ with $T_w > T_\infty$. By following [1–3], the mathematical formulation is expressed as:

$$\frac{\partial(\bar{r}u)}{\partial \bar{x}} + \frac{\partial(\bar{r}v)}{\partial \bar{y}} = 0 \tag{1}$$

$$\bar{u}\frac{\partial \bar{u}}{\partial \bar{x}} + \bar{v}\frac{\partial \bar{u}}{\partial \bar{y}} = \nu \frac{\partial^2 \bar{u}}{\partial \bar{y}^2} + g\frac{\rho - \rho_\infty}{\rho_\infty}\sin\frac{\bar{x}}{a} - \frac{\sigma B_0^2}{\rho}u \tag{2}$$

$$\bar{u}\frac{\partial T}{\partial \bar{x}} + \bar{v}\frac{\partial T}{\partial \bar{y}} = \alpha_m \frac{\partial^2 T}{\partial \bar{y}^2} - \frac{1}{\rho C_p}\frac{\partial q_r}{\partial y} \tag{3}$$
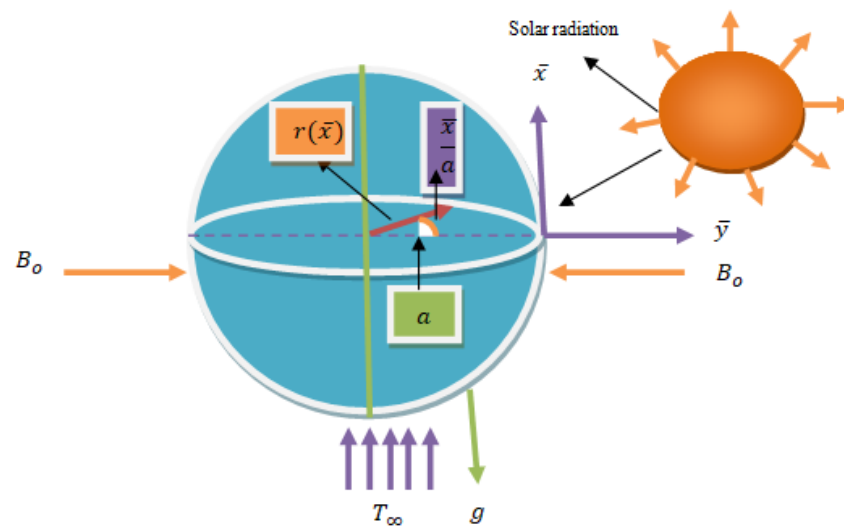
Figure 1. Flow Geometry and Coordinate System.

The distance from the symmetric axis to the sphere surface is $\bar{r} = a\ \sin\frac{\bar{x}}{a}$ and is known as radial distance. The notations $(\bar{u}, \bar{v})$ are velocity components toward and normal to the flow direction. The symbols a, g, ρ, ν, σ_e, B_0 and α_m designate the radius of the sphere, gravity acceleration, fluid density, kinematic viscosity, electric conductivity, thermal diffusivity and magnetic field strength, respectively.

Below is a presentation of the radiant heat flow q_r:

$$qr = -4\sigma 3KR\partial T4\partial y. \tag{4}$$

K_R stands for mean absorption coefficient. Stefan–Boltzmann constant is represented by the symbol σ. Equation (4)'s right side T^4 is given as follows.

$$\mathrm{T}^4 \approx 4\mathrm{T}_\infty^3\mathrm{T} - 3\mathrm{T}_\infty^4.$$

So, Equation (4) becomes:

$$q_r = -\frac{16T_\infty^3\sigma}{3K_R}\frac{\partial T}{\partial y} \tag{5}$$

and Equation (3) is expressed as:

$$u\frac{\partial T}{\partial x} + v\frac{\partial T}{\partial y} = \frac{k_\infty}{\rho C_p}\frac{\partial^2 T}{\partial y^2} + \frac{16T_\infty^3\sigma}{\rho C_P 3K_R}\frac{\partial^2 T}{\partial y^2} \tag{6}$$

Further simplification of Equation (6) gives:

$$u\frac{\partial T}{\partial x} + v\frac{\partial T}{\partial y} = \frac{k}{\rho C_p}\frac{\partial}{\partial y}\left[\frac{\partial T}{\partial y} + \frac{4.4\ T_\infty^3\sigma}{\rho C_P 3kK_R}\frac{\partial T}{\partial y}\right] \tag{7}$$

The relationship between density and temperature is as follows:

$$\frac{\rho - \rho_m}{\rho_m} = -\gamma(T - T_m)^2 \tag{8}$$

Furthermore, Equation (6) implies that for steady flow:

$$T \to T_m \pm \Delta Ty \to \pm\infty \tag{9}$$

For fixed ΔT. Consider region $y \geq 0$ subject to the boundary conditions to obtain the symmetry in this situation.

$$\bar{u} = 0, \ \bar{v} = 0, \ \ T = T_m \text{ at } y = 0 \, \bar{u} \rightarrow 0, \ T \rightarrow T_\infty \ \text{as } y \rightarrow \infty \tag{10}$$

where $T_\infty = T + \Delta T$ and has the relation with ρ_∞ shown by Equation (8). Determining the reduced gravity is simple.

$$g' = g \frac{(\rho_m - \rho_\infty)}{\rho_\infty} \tag{11}$$

Fluid particle acceleration has a density ρ_m. Thus, from Equation (8):

$$g' = g\gamma \frac{\rho_m}{\rho_\infty}(T_\infty - T_m)^2 \tag{12}$$

Moreover, skin friction coefficient and Nusselt number at the surface are expressed as follows:

$$C_f = \frac{\tau_w}{\rho U^2}, \ Nu = \frac{xq_w}{k(T_w - T_\infty)} \tag{13}$$

$$\text{where } \tau_w = \mu\left(\frac{\partial \bar{u}}{\partial \bar{y}}\right)_{\bar{y}=0}, \ \ q_w = -k\left(\frac{\partial T}{\partial \bar{y}}\right)_{\bar{y}=0}, \tag{14}$$

3. Dimensionless Variables

The equations given in (1)–(3) subject to conditions given in (10) are made dimensionless by employing the following non-dimensional variables [9]:

$$x = \frac{\bar{x}}{a}, \ y = \frac{\bar{y}Gr^{\frac{1}{4}}}{a}, \theta = \frac{T - T_\infty}{T_m - T_\infty}, \ u = \frac{a\bar{u}Gr^{\frac{1}{4}}}{\nu}, v = \frac{a\bar{v}Gr^{\frac{1}{4}}}{\nu}, \tag{15}$$

By introducing Equation (10) into Equations (1)–(3) with (8) we have,

$$\frac{\partial(\sin xu)}{\partial x} + \frac{\partial(\sin xv)}{\partial y} = 0, \tag{16}$$

$$u\frac{\partial u}{\partial x} + v\frac{\partial u}{\partial y} = \frac{\partial^2 u}{\partial y^2} + R_g\left(2\theta - \theta^2\right)\sin x - Mu \tag{17}$$

$$u\frac{\partial \theta}{\partial x} + v\frac{\partial \theta}{\partial y} = \frac{1}{Pr}\left(1 + \frac{4}{3}Rd\right)\frac{\partial^2 \theta}{\partial y^2}, \tag{18}$$

$$\begin{array}{c} u = 0, \ v = 0, \ \ \theta = 1, \text{ at } y = 0 \\ u \rightarrow 0, \ \ \theta \rightarrow 0, \ \ \text{ as } y \rightarrow \infty. \end{array} \tag{19}$$

Here, $R_g = \frac{g'}{g\,\beta\Delta T}$, $Rd = kK_R/4\sigma^* T_\infty^3$, $Pr = \frac{\nu}{\alpha}$ and $M = \frac{\sigma B_o^2 a^2 Gr^{\frac{1}{4}}}{\rho\nu}$ are reduced gravity, radiation parameter, Prandtl number, and magnetic field parameter, respectively. Here, g' is reduced gravity acceleration defined in Equation (12).

4. Solution Methodology

The above Equations (16)–(19) are discretized using the finite difference method. Theses equations are firstly transformed to a smooth form, then a numerical algorithm is written using FORTRAN coding language. The dimensionless variables are defined as [9]:

$$u(x,y) = x^{1/2}U(X,Y), \ v(x,y) = x^{-\frac{1}{4}}V(X,Y), Y = x^{-\frac{1}{4}}y, \ X = x, \ \theta(x,y) = \theta(X,Y) \tag{20}$$

By putting Equation (20) in (16)–(19) the set of governing equations becomes:

$$\text{X}U \, \cos X + \left(X \frac{\partial U}{\partial X} - \frac{Y}{2} \frac{\partial U}{\partial Y} + \frac{\partial V}{\partial Y} \right) \sin X = 0, \tag{21}$$

$$XU \frac{\partial U}{\partial X} + \frac{1}{2} U^2 + \left(V - \frac{YU}{2} \right) \frac{\partial U}{\partial Y} = \frac{\partial^2 U}{\partial Y^2} + Rg \left(2\theta - \theta^2 \right) \sin X - MU \tag{22}$$

$$XU \frac{\partial \theta}{\partial X} + \left(V - \frac{YU}{2} \right) \frac{\partial \theta}{\partial Y} = \frac{1}{Pr} \left(1 + \frac{4}{3} Rd \right) \frac{\partial^2 \theta}{\partial Y^2} \tag{23}$$

The corresponding boundary conditions are:

$$\begin{aligned} U = 0 \,, \ V = 0, \ \theta = 1, \ \text{at } Y = 0 \\ U \to 0 \,, \theta \to 0, \ \text{as } Y \to \infty. \end{aligned} \tag{24}$$

Method of Solution

The finite difference method is used to solve the set of governing Equations (21)–(23) with the boundary conditions (24). The X-axis is used to apply the backward difference, while the Y-axis is used to apply the central difference. After the discretization of the governing equations, the discretized variables are identified as $(U_{i,j}, V_{i,j}, \theta_{i,j})$. The detailed discretization is described as follow:

$$\frac{\partial U}{\partial X} = \frac{U_{(i,j)} - U_{(i,j-1)}}{\Delta X} \tag{25}$$

$$\frac{\partial U}{\partial Y} = \frac{U_{(i+1,j)} - U_{(i-1,j)}}{2\Delta Y} \tag{26}$$

$$\frac{\partial^2 U}{\partial Y^2} = \frac{U_{(i+1,j)} - 2U_{(i,j)} + U_{(i,-1,j)}}{\Delta Y^2} \tag{27}$$

The following system of algebraic equations is obtained by combining Equations (25)–(27), Equations (21)–(23), and the boundary conditions specified in Equation (24).

Continuity equation:

$$\begin{aligned} V_{(i+1,j)} = V_{(i-1,j)} - 2\frac{\Delta Y}{\Delta X} X_i \left(U_{(i,j)} - U_{(i,j-1)} \right) + \frac{Y_j}{2} \left(U_{(i+1,j)} - U_{(i-1,j)} \right) \\ -2\Delta Y X_i \frac{\cos X_i}{\sin X_i} U_{(i,j)}, \end{aligned} \tag{28}$$

Momentum equation:

$$\begin{aligned} \left(1 + \frac{\Delta Y}{2} \left(V_{(i,j)} - \frac{Y_j}{2} U_{(i,j)} \right) \right) U_{(i-1,j)} + \left(-2 - \frac{\Delta Y^2}{\Delta X} X_i U_{(i,j)} - M \right) U_{(i,j)} + \\ \left(1 - \frac{\Delta Y}{2} \left(V_{(i,j)} - \frac{Y_j}{2} U_{(i,j)} \right) \right) U_{(i+1,j)} = -\Delta Y^2 \sin X_i Rg (2\theta_{(i,j)} - \theta^2{}_{(i,j)}) \end{aligned} \tag{29}$$

Energy equation:

$$\begin{aligned} \left(\frac{1}{Pr} \left(1 + \frac{4}{3} Rd \right) + \frac{\Delta Y}{2} \left(V_{(i,j)} - \frac{Y_j}{2} U_{(i,j)} \right) \right) \theta_{(i-1,j)} + \left(-\frac{2}{Pr} \left(1 + \frac{4}{3} Rd \right) + \\ \Delta Y^2 U_{(i,j)} \left(1 - \frac{X_i}{\Delta X} \right) \right) \theta_{(i,j)} + \left(\frac{1}{Pr} \left(1 + \frac{4}{3} Rd \right) - \frac{\Delta Y}{2} \left(V_{(i,j)} - \frac{Y_j}{2} U_{(i,j)} \right) \right) \theta_{(i+1,j)} = \\ -\frac{\Delta Y^2}{\Delta X} X_i U_{(i,j)} \theta_{(i,j-1)} \end{aligned} \tag{30}$$

The convergence criterion is presented as follows to achieve accurate numerical solutions for the variables U, V and θ, respectively.

$$\max \left| U_{ij} \right| + \max \left| V_{ij} \right| + \max \left| \theta_{ij} \right| \leq \epsilon$$

where $\epsilon = 10^{-5}$. The computation is started at $X = 0$ and then marches downstream implicitly.

5. Grid Independency Test and Numerical Model Verification

To check the accuracy of the numerical model a grid independency test is performed by considering different grid numbers. The grid independency test is performed for $M = 1.0$, $Rd = 1.0$, $R_g = 5.0$ and $Pr = 7.0$ at the circumferential position $X = \pi/4$. The results of this test are presented in Table 1. It is noticed that an excellent solution accuracy is observed as the number of grid points is increased. The deviation between 200 point and 500-point grids for the skin friction and heat transfer rate at position $X = \pi/4$ are calculated. It is noticed that deviation percentages are 0.09% and 0.003% for skin friction and heat transfer rate, respectively. Thus, the 200-point grid can be considered as sufficient for the convergence and accuracy of the results and is chosen to perform all the calculations. This grid corresponds to step sizes $\Delta X = 0.05$ and $\Delta Y = 0.02$. The solutions determined using the finite difference method based on the selected grid are discussed in detail in the forthcoming section.

Table 1. Grid independency test for $M = 1.0$, $Rd = 1.0$, $R_g = 10.0$, and $Pr = 7.0$ at $X = \pi/4$.

No. of Grid Points	$\left(\frac{\partial U}{\partial Y}\right)_{Y=0}$	$-\left(\frac{\partial \theta}{\partial Y}\right)_{Y=0}$
25.0	2.01299	0.79793
50.0	2.12478	0.77268
100.0	2.15249	0.76919
200.0	2.15950	0.76891
250.0	2.16036	0.76892
500.0	2.16150	0.76894

In order to verify the validity of the proposed numerical model, a comparison of the findings of $\left(\frac{\partial U}{\partial Y}\right)_{Y=0}$ with earlier published results for several Pr values are presented in Table 2. In can be noticed that a good concordance exists between the results.

Table 2. Verification of numerical model; comparison of $\left(\frac{\partial U}{\partial Y}\right)_{Y=0}$ with the results of Sparrow & Gregg [26] in the absence of the reduced gravity term for $M = 0$ and $Rd = 0$, at $\pi/2$.

Pr	Sparrow & Gregg [26]	Present
0.03	0.93841	0.93740
0.02	0.95896	0.95870
0.008	0.99550	0.99400

6. Results and Discussion

In current section the numerical solutions of the set of the equations governing the considered configuration are discussed in detail. The effects of the parameters governing the studied configuration on the velocity U, and temperature θ, profiles in addition to the coefficient of skin friction C_f and the Nusselt number Nu are presented in form of graphs and tables. Figure 2 depicts the effect of the reduced gravity parameter Rg on the velocity profile U for Prandtl number $Pr = 7.0$ at different locations of the sphere. It is noticed that at diverse positions of the sphere when Rg is increased, the fluid velocity increases. In Figure 3 the numerical outcomes of temperature θ for different values of Rg are displayed. The temperature curves show that at higher Rg values, the fluid temperature drops quickly at all the considered positions. From physical point of view the trend of temperature is logical because the intensification in reduced gravity parameter leads to

a reduction in thermal expansion and temperature difference between the surface and ambient temperature, and hence the overall temperature of the fluid flow domain decreases. However, the maximum magnitude for temperature is attained at $X = \pi$. The velocity profiles for several Pr values are sketched in Figure 4. It is remarked that the increase of Pr leads to a reduction of the fluid velocity at all the considered positions. This decrease is due to increase of the fluid viscosity that causes the increase of the viscous effect and hence the decrease of flow intensity. It is also to be mentioned that the highest value for U is achieved at $X = \frac{\pi}{2}$. Figure 5 shows the effects of Pr on the temperature profiles. Graphical outcomes indicate that the temperature of the fluid reduces as Pr is enhanced. From physical point of this is due to the decrease of the thermal conductivity when Pr is increased. In fact, the capability of the fluid to conduct the heat is reduced and thus the temperature of the fluid decreases. Figures 6 and 7 show the behaviors of velocity and temperature profiles for several values of radiation parameter Rd at several positions around the sphere. It is noticed that temperature and fluid velocity rise with the augmenting numerical of Rd values. An intensification in Rd leads to a rise the thermal conductance of the fluid and the mean absorption coefficient that helps to boost the temperature of the fluid flow as shown in Figures 6 and 7. Figures 8 and 9 illustrate the impact of magnetic field parameter M on the temperature and velocity profiles. It is to be mentioned that the velocity is decreasing, and the temperature is increasing with the intensification of the magnitude of the magnetic field. From a physical point of view, the application of the external applied magnetic field perpendicular to the flow direction generates a Lorentz force that opposes the flow and reduce the fluid velocity. In addition, due to the resistance to the flow, the viscous effect causes an augmentation of fluid temperature. Table 3 presents the results of the of skin friction coefficient and Nusselt number versus the reduced gravity parameter Rg. An increasing in the values of Rg enhances the skin friction coefficient and Nusselt number at all the considered circumferential positions.
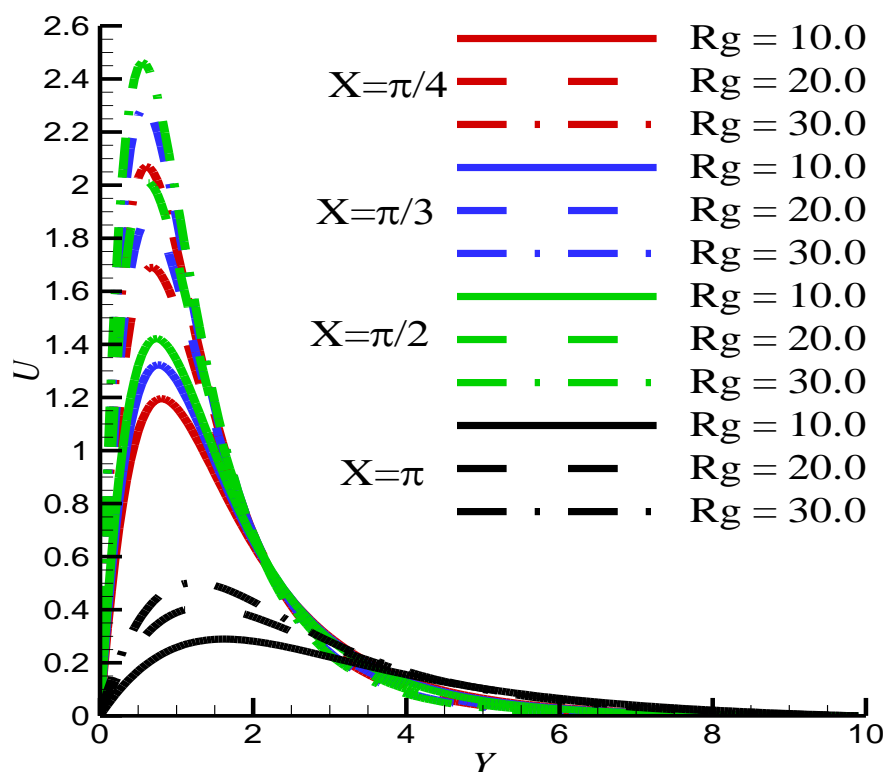

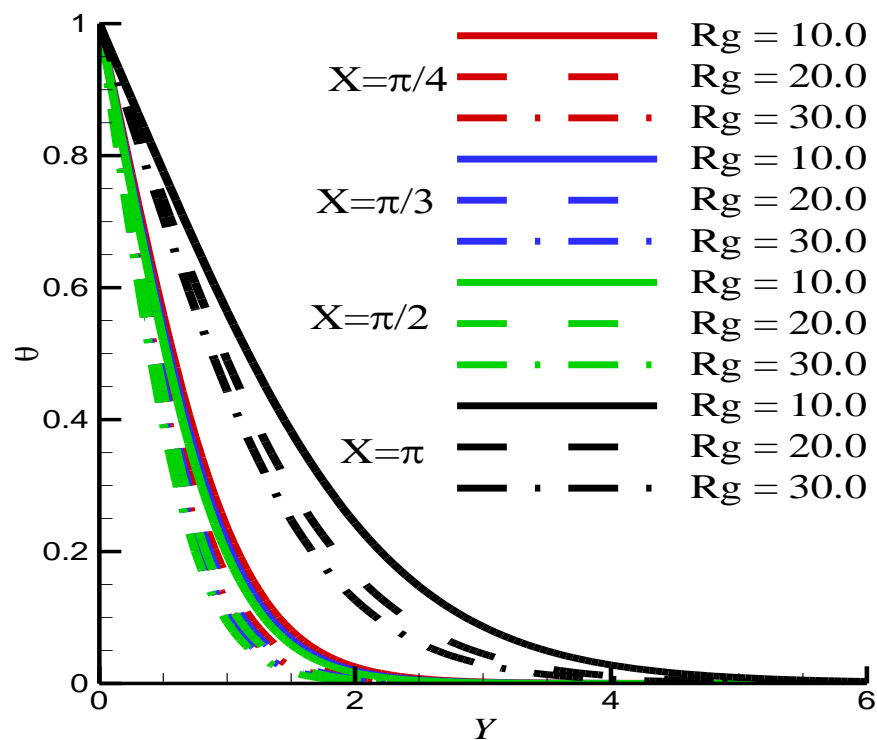**Figure 2.** Effect of Rg on θ for $Pr = 7.0$, $Rd = 1.0$, and $M = 1.0$.

Figure 3. Effect of *Rg* on *U* for *Pr* = 7.0, *Rd* = 1.0, and *M* = 1.0.
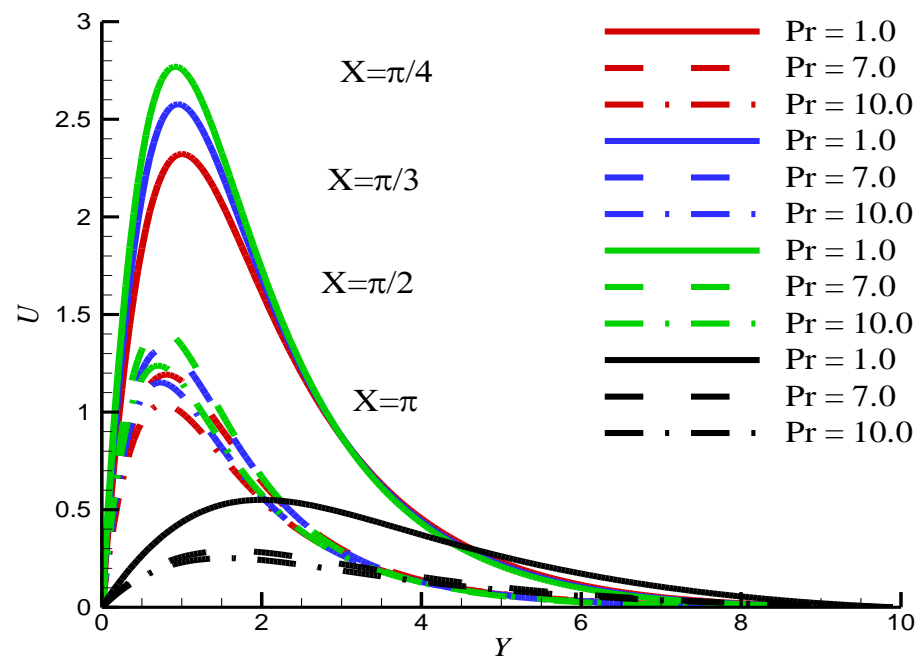
Figure 4. Effect of *Pr* on *U* for *Rg* = 10.0, *Rd* = 1.0, and *M* = 1.0.
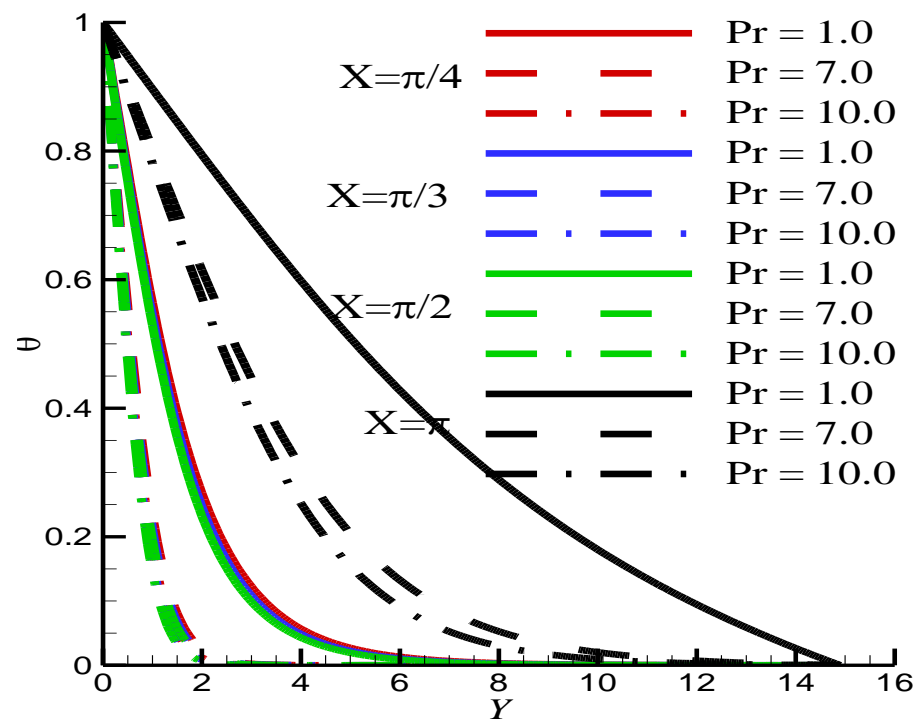
Figure 5. Effect of *Pr* on θ for *Rg* = 10.0, *Rd* = 1.0, and *M* = 1.0.
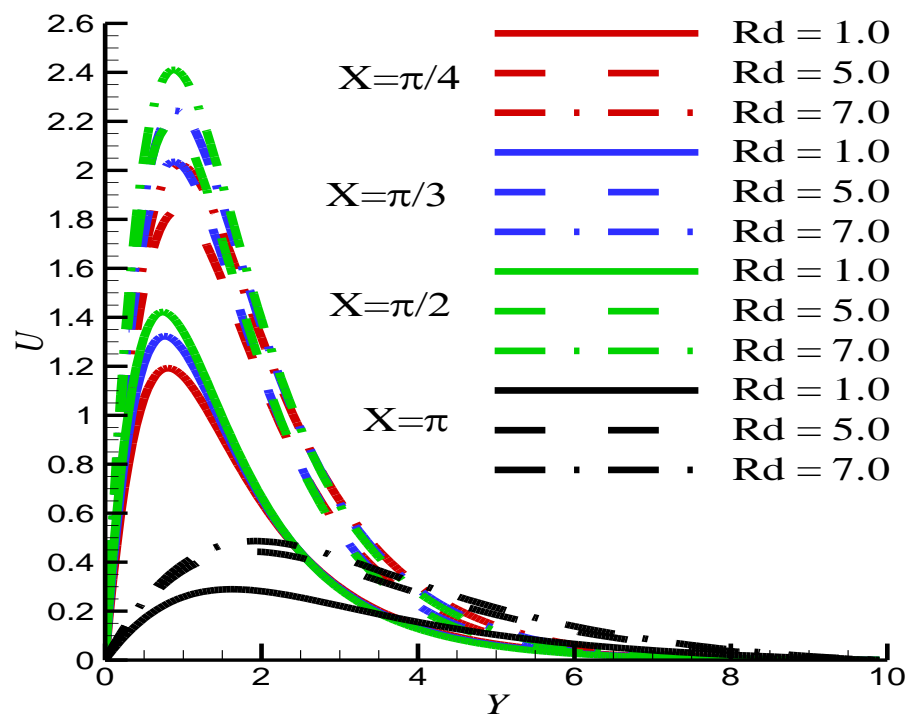
Figure 6. Effect of *Rd* on *U* for *Rg* = 10.0, *Pr* = 7.0, and *M* = 1.0.
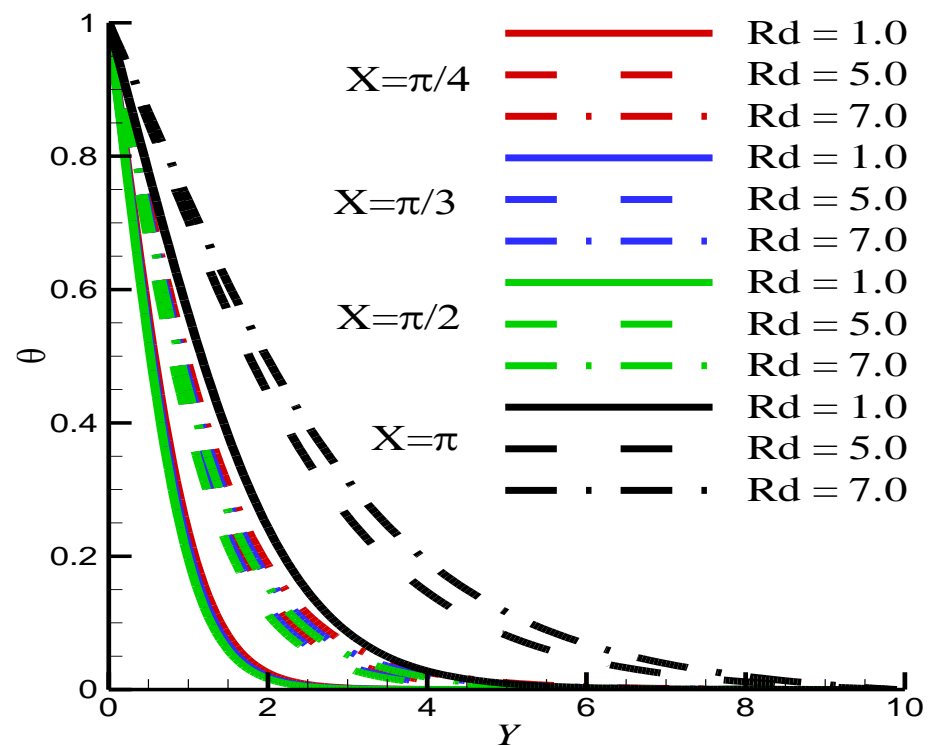
Figure 7. Effect of *Rd* on θ for *Rg* = 10.0, *Pr* = 7.0, and *M* = 1.0.
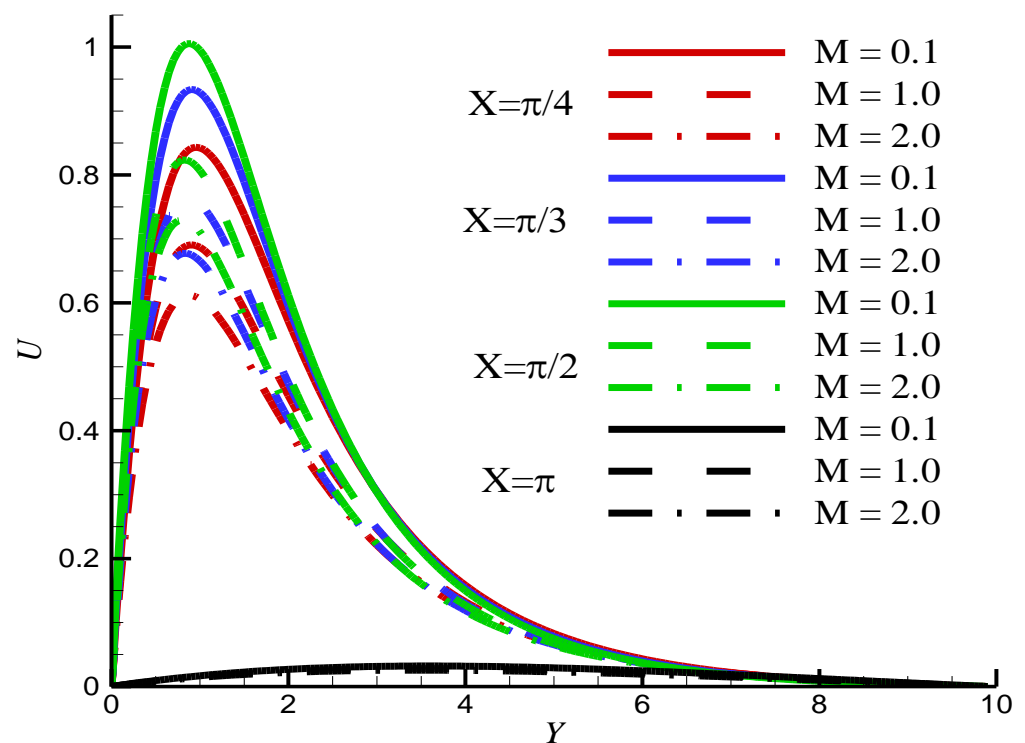
Figure 8. Effect of *M* on *U* for *Rg* = 5.0, *Pr* = 7.0, *Rd* = 1.0, and *M* = 1.0.
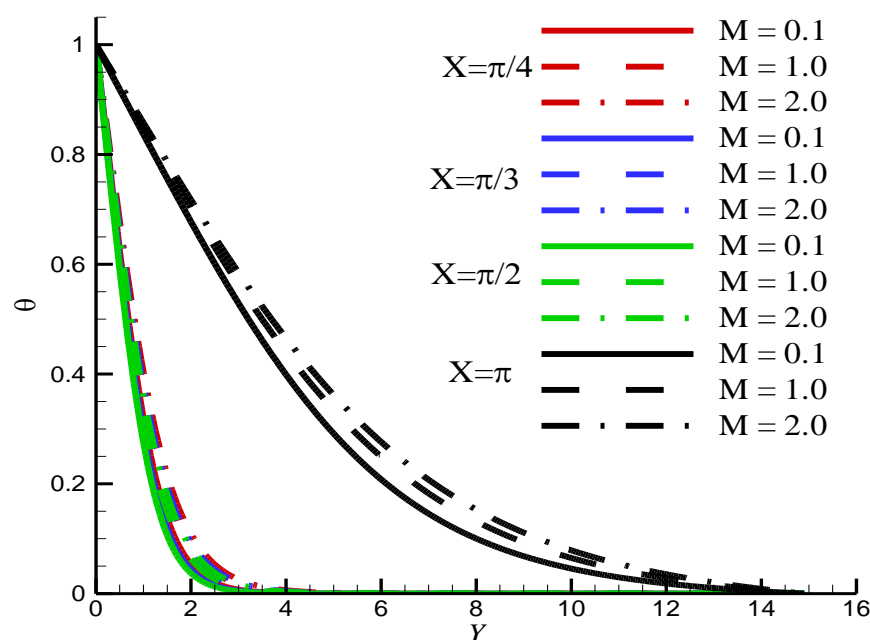
Figure 9. Effect of M on θ for Rg = 5.0, Pr = 7.0, Rd = 1.0, and M = 1.0.

Table 3. Consequences of reduced gravity parameter Rg on kin friction coefficient C_f and Nusselt number Nu.

	C_f				Nu			
X	Rg = 0.1	Rg = 1.0	Rg = 5.0	Rg = 10.0	Rg = 0.1	Rg = 1.0	Rg = 5.0	Rg = 10.0
$\pi/6$	0.10860	0.64508	2.16368	3.63897	0.16210	0.28475	0.42706	0.50809
$\pi/4$	0.14868	0.86768	2.90589	4.886676	0.17741	0.31446	0.47131	0.56063
$\pi/2$	0.19412	1.12016	3.74840	6.30307	0.19241	0.34257	0.51314	0.61033
π	0.00013	0.00135	0.00701	0.01477	0.10090	0.09991	0.09515	0.08816

7. Conclusions

In the current study, the effects of reduced gravity, solar radiation, and external magnetic field on the natural convection past a stationary sphere immersed in a fluid are investigated. The main findings related to effects of reduced gravity and Prandtl number on the velocity U, temperature θ, skin friction coefficient C_f, and Nusselt number Nu are summarized as:

- When Rg is increased, the velocity increases, and the temperature decreases due the enhancement of the buoyancy force.
- The increase of Pr leads to the decrease of the velocity and temperature of the fluid, due to the increase of the viscosity.
- The application of an external magnetic field causes the reduction of the flow intensity and an augmentation of the temperature.
- The increase in Rd cause an increase of the temperature and a reduction of the velocity.

Author Contributions: Conceptualization, A.A. and M.A.; methodology, A.A.; software, M.A.; validation, I.E.S., K.G. and T.L.; formal analysis, A.A.; investigation, L.K.; resources, K.G.; data curation, H.A.; writing—original draft preparation, A.A.; writing—review and editing, H.A.; visualization, L.K.; supervision, M.A; project administration, K.G.; funding acquisition, K.G. All authors have read and agreed to the published version of the manuscript.

References

1. Potter, J.M.; Riley, N. Free convection from a heated sphere at large Grashof number. *J. Fluid Mech.* **1980**, *100*, 769–783. [CrossRef]
2. Riley, N. The heat transfer from a sphere in free convective flow. *Comput. Fluids* **1986**, *14*, 225–237. [CrossRef]
3. Kay, A.; Kuiken, H.K.; Merkin, J.H. Boundary-layer analysis of the thermal bar. *J. Fluid Mech.* **1995**, *303*, 253–278. [CrossRef]
4. Ashraf, M.; Fatima, A.; Gorla, R.S.R. Periodic momentum and thermal boundary layer mixed convection flow around the surface of a sphere in the presence of viscous dissipation. *Can. J. Phys.* **2017**, *95*, 976–986. [CrossRef]
5. Ashraf, M.; Fatima, A. Numerical simulation of the effect of transient shear stress and the rate of heat transfer around different positions of sphere in the presence of viscous dissipation. *J. Heat Transf.* **2018**, *140*, 701–702. [CrossRef]
6. Ashraf, M.; Khan, A.; Gorla, R.S.R. Natural convection boundary layer flow of nanofluids around different stations of the sphere and into the plume above the sphere. *Heat Transf. Asian Res.* **2019**, *48*, 1127–1148. [CrossRef]
7. Abbas, A.; Ashraf, M.; Chu, Y.; Zia, S.; Khan, I.; Nisar, K.S. Computational Study of the Coupled Mechanism of Thermophoretic Transportation and Mixed Convection Flow around the Surface of a Sphere. *Molecules* **2020**, *25*, 2694. [CrossRef] [PubMed]
8. Abbas, A.; Muhammad, A. Combined effects of variable viscosity and thermophoretic transportation on mixed convection flow around the surface of a sphere. *Therm. Sci.* **2020**, *24*, 4089–4101. [CrossRef]
9. Ashraf, M.; Abbas, A.; Ali, A.; Shah, Z.; Alrabaiah, H.; Bonyah, E. Numerical simulation of the combined effects of thermophoretic motion and variable thermal conductivity on free convection heat transfer. *AIP Adv.* **2020**, *10*, 085005. [CrossRef]
10. Abbas, A.; Ashraf, M.; Chamkha, A.J. Combined effects of thermal radiation and thermophoretic motion on mixed convection boundary layer flow. *Alex. Eng. J.* **2021**, *60*, 3243–3252. [CrossRef]
11. Ashraf, M.; Abbas, A.; Zia, S.; Chu, Y.M.; Khan, I.; Nisar, K.S. Computational analysis of the effect of nano particle material motion on mixed convection flow in the presence of heat generation and absorption. *CMC Comput. Mater. Contin.* **2020**, *65*, 1809–1823. [CrossRef]
12. Ashraf, M.; Abbas, A.; Oztop, H.F.; Nisar, K.S.; Khan, I. Computations of mixed convection slip flow around the surface of a sphere: Effects of thermophoretic transportation and viscous dissipation. *Heat Transf.* **2021**, *50*, 7349–7362. [CrossRef]
13. Ahmad, U.; Ashraf, M.; Abbas, A.; Rashad, A.M.; Nabwey, H.A. Mixed convection flow along a curved surface in the presence of exothermic catalytic chemical reaction. *Sci. Rep.* **2021**, *11*, 12907. [CrossRef] [PubMed]
14. Abbas, A.; Ijaz, I.; Ashraf, M.; Ahmad, H. Combined effects of variable density and thermal radiation on MHD Sakiadis flow. *Case Stud. Therm. Eng.* **2021**, *28*, 101640. [CrossRef]
15. Rashad, A.M.; Chamkha, A.J.; Modather, M. Mixed convection boundary-layer flow past a horizontal circular cylinder embedded in a porous medium filled with a nanofluid under convective boundary conditions. Comput. *Fluids* **2013**, *86*, 380–388. [CrossRef]
16. Khan, A.; Ashraf, M.; Rashad, A.M.; Nabwey, H.A. Impact of Heat Generation on Magneto Nanofluid Free Convection Flow About Sphere In The Plume Region. *Mathematics* **2020**, *8*, 2010. [CrossRef]
17. Bulinda, V.M.; Kang'ethe, G.P.; Kiogora, P.R. Magnetohydrodynamics Free Convection Flow of Incompressible Fluids over Corrugated Vibrating Bottom Surface with Hall Currents and Heat and Mass Transfers. *J. Appl. Math.* **2020**, *2020*, 2589760. [CrossRef]
18. Molla, M.M.; Rahman, A.; Rahman, L.T. Natural convection flow from an isothermal sphere with temperature dependent thermal conductivity. *J. Nav. Archit. Mar. Eng.* **2005**, *2*, 53–64. [CrossRef]
19. Alwawi, F.A.; Alkasasbeh, H.T.; Rashad, A.M.; Idris, R. MHD natural convection of Sodium Alginate Casson nanofluid over a solid sphere. *Results Phys.* **2020**, *16*, 102818. [CrossRef]
20. Jenifer, A.S.; Saikrishnan, P.; Lewis, R.W. Unsteady MHD Mixed Convection Flow of Water over a Sphere with Mass Transfer. *J. Appl. Comput. Mech.* **2021**, *7*, 935–943.
21. Ahmad, U.; Ashraf, M.; Al-Zubaidi, A.; Ali, A.; Saleem, S. Effects of temperature dependent viscosity and thermal conductivity on natural convection flow along a curved surface in the presence of exothermic catalytic chemical reaction. *PLoS ONE* **2021**, *16*, e0252485. [CrossRef]
22. Salleh, M.Z.; Nazar, R.; Pop, I. Mixed convection boundary layer flow about a solid sphere with Newtonian heating. *Arch. Mech.* **2010**, *62*, 283–303.
23. Molla, M.; Hossain, A. Effects of chemical reaction, heat and mass diffusion in natural convection flow from an isothermal sphere with temperature dependent viscosity. *Eng. Comput.* **2006**, *23*, 840–857. [CrossRef]
24. Chamkha, A. Non-Darcy natural convection of a nanofluid about a permeable vertical cone embedded in a porous medium. *Int. J. Microscale Nanoscale Therm.* **2012**, *4*, 99–114.
25. Chamkha, A.J.; Aly, A.M.; Raizah, Z.A.S. Double-Diffusion MHD free convective flow along a sphere in the presence of a homogeneous chemical reaction and Soret and Dufour effects. *Appl. Comput. Math.* **2017**, *6*, 34. [CrossRef]
26. Sparrow, E.M.; Gregg, J.L. *Details of Exact Low Prandtl Number Boundary-Layer Solutions for Forced and for Free Convection*; No. NASA-MEMO-2-27-59E; NASA: Washington, DC, USA, 1959.

27. Zhang, L.; Zhang, X.; Peng, S.; Yan, Z.; Liang, Y.; Yan, B.; Li, Q. Thermal-mechanical coupling propagation and transient thermal fracture in multilayer coatings. *Heat Transf. Res.* **2017**, *48*, 935–954. [CrossRef]

28. Liu, L.; Li, Q.; Ju, F.; Dong, X.; Yu, X. Numerical simulation and analysis of the vertical and double pipe soil-air heat exchanger. *Therm. Sci.* **2019**, *23*, 3905–3916. [CrossRef]

29. Ali, L.; Ali, B.; Ghori, M.B. Melting effect on Cattaneo–Christov and thermal radiation features for aligned MHD nanofluid flow comprising microorganisms to leading edge: FEM approach. *Comput. Math. Appl.* **2022**, *109*, 260–269. [CrossRef]

30. Ali, L.; Ali, B.; Liu, X.; Ahmed, S.; Shah, M.A. Analysis of bio-convective MHD Blasius and Sakiadis flow with Cattaneo-Christov heat flux model and chemical reaction. *Chin. J. Phys.* **2022**, *77*, 1963–1975. [CrossRef]

31. Ali, L.; Ali, B.; Liu, X.; Iqbal, T.; Zulqarnain, R.M.; Javid, M. A comparative study of unsteady MHD Falkner–Skan wedge flow for non-Newtonian nanofluids considering thermal radiation and activation energy. *Chin. J. Phys.* **2022**, *77*, 1625–1638. [CrossRef]

32. Ali, L.; Wang, Y.; Ali, B.; Liu, X.; Din, A.; Al Mdallal, Q. The function of nanoparticle's diameter and Darcy-Forchheimer flow over a cylinder with effect of magnetic field and thermal radiation. *Case Stud. Therm. Eng.* **2021**, *28*, 101392. [CrossRef]

33. Abbas, A.; Ahmad, H.; Mumtaz, M.; Ilyas, A.; Hussan, M. MHD dissipative micropolar fluid flow past stretching sheet with heat generation and slip effects. *Waves Random Complex Media* **2022**, 1–15. [CrossRef]

34. Abbas, A.; Jeelani, M.B.; Alnahdi, A.S.; Ilyas, A. MHD Williamson Nanofluid Fluid Flow and Heat Transfer Past a Non-Linear Stretching Sheet Implanted in a Porous Medium: Effects of Heat Generation and Viscous Dissipation. *Processes* **2022**, *10*, 1221. [CrossRef]

35. Abbas, A.; Shafqat, R.; Jeelani, M.B.; Alharthi, N.H. Significance of Chemical Reaction and Lorentz Force on Third-Grade Fluid Flow and Heat Transfer with Darcy–Forchheimer Law over an Inclined Exponentially Stretching Sheet Embedded in a Porous Medium. *Symmetry* **2022**, *14*, 779. [CrossRef]

36. Abbas, A.; Jeelani, M.B.; Alharthi, N.H. Darcy–Forchheimer Relation Influence on MHD Dissipative Third-Grade Fluid Flow and Heat Transfer in Porous Medium with Joule Heating Effects: A Numerical Approach. *Processes* **2022**, *10*, 906. [CrossRef]

37. Abbas, A.; Noreen, A.; Ali, M.A.; Ashraf, M.; Alzahrani, E.; Marzouki, R.; Goodarzi, M. Solar radiation over a roof in the presence of temperature-dependent thermal conductivity of a Casson flow for energy saving in buildings. *Sustain. Energy Technol. Assess.* **2022**, *53*, 102606. [CrossRef]

38. Abbas, A.; Jeelani, M.B.; Alharthi, N.H. Magnetohydrodynamic Effects on Third-Grade Fluid Flow and Heat Transfer with Darcy–Forchheimer Law over an Inclined Exponentially Stretching Sheet Embedded in a Porous Medium. *Magnetochemistry* **2022**, *8*, 61. [CrossRef]

39. Abbas, A.; Shafqat, R.; Jeelani, M.B.; Alharthi, N.H. Convective Heat and Mass Transfer in Third-Grade Fluid with Darcy–Forchheimer Relation in the Presence of Thermal-Diffusion and Diffusion-Thermo Effects over an Exponentially Inclined Stretching Sheet Surrounded by a Porous Medium: A CFD Study. *Processes* **2022**, *10*, 776. [CrossRef]

40. Ashraf, M.; Ilyas, A.; Ullah, Z.; Abbas, A. Periodic magnetohydrodynamic mixed convection flow along a cone embedded in a porous medium with variable surface temperature. *Ann. Nucl. Energy* **2022**, *175*, 109218. [CrossRef]

41. Ullah, Z.; Bilal, M.; Sarris, I.E.; Hussanan, A. MHD and Thermal Slip Effects on Viscous Fluid over Symmetrically Vertical Heated Plate in Porous Medium: Keller Box Analysis. *Symmetry* **2022**, *14*, 2421. [CrossRef]

42. Bhatti, M.M.; Shahid, A.; Sarris, I.E.; Bég, O.A. Spectral relaxation computation of Maxwell fluid flow from a stretching surface with quadratic convection and non-Fourier heat flux using Lie symmetry transformations. *Int. J. Mod. Phys. B* **2022**, *37*, 2350082. [CrossRef]

43. Maranna, T.; Sneha, K.N.; Mahabaleshwar, U.S.; Sarris, I.E.; Karakasidis, T.E. An Effect of Radiation and MHD Newtonian Fluid over a Stretching/Shrinking Sheet with CNTs and Mass Transpiration. *Appl. Sci.* **2022**, *12*, 5466. [CrossRef]

44. Punith Gowda, R.J.; Sarris, I.E.; Naveen Kumar, R.; Kumar, R.; Prasannakumara, B.C. A Three-Dimensional Non-Newtonian Magnetic Fluid Flow Induced Due to Stretching of the Flat Surface with Chemical Reaction. *J. Heat Transf.* **2022**, *144*, 113602. [CrossRef]

45. Ullah, Z.; Ashraf, M.; Sarris, I.E.; Karakasidis, T.E. The Impact of Reduced Gravity on Oscillatory Mixed Convective Heat Transfer around a Non-Conducting Heated Circular Cylinder. *Appl. Sci.* **2022**, *12*, 5081. [CrossRef]